Novel Rare-Earth-Containing Lead-Free Solders with Enhanced Ductility

M.A. Dudek, R.S. Sidhu, and N. Chawla

Several lead-free material systems are available as replacements for traditional lead-based solders in microelectronic packaging, including near-eutectic combinations of tin-rich alloys. Although these materials have superior mechanical properties as compared to the Pb-Sn system, much work remains in developing these materials for electronic packaging. Small additions of rare-earth elements have been shown to refine the microstructure of several lead-free solder systems, thus improving their mechanical properties. This study investigated the effect of the addition of lanthanum on the melting behavior, microstructure, and shear strength of an Sn-3.9Ag-0.7Cu alloy. The influence of $LaSn_3$ intermetallics on microstructural refinement and damage evolution in these novel solders is discussed.

INTRODUCTION

Global concern over the environmental impact and health effects of lead-based solders in consumer electronics has led to the development of lead-free solder alternatives. Sn-Ag-Cu is one of the most promising lead-free alloys for replacement of Pb-Sn solder.[1] It is superior to other tin-rich alloys because of its relatively low melting temperature, superior mechanical properties, good solderability, and relatively low cost.[2] Although these materials are, in principle, suitable as replacements for Pb-Sn,[1] many issues still need to be addressed. These include a higher soldering temperature compared to Pb-Sn compositions, and, in particular, lower ductility.[3,4] The lower ductility of the solder has important implications because it is directly related to mechanical shock and drop resistance.[5]

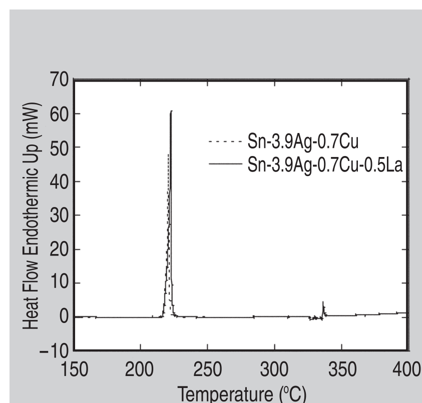

Figure 1. The heat flow vs. temperature curve for Sn-3.9Ag-0.7Cu and Sn-3.9Ag-0.7Cu-0.5La heating cycles.

Table I. Summary of Microstructural Characterization Results for As-Processed Solder Alloys

	Concentration of La (wt.%)		
	0	0.1	0.5
$LaSn_3$ Characteristics			
Volume Fraction (%)	N/A	0.8 ± 0.1	2.4 ± 0.2
Major Axis (μm)	N/A	2.7 ± 0.1	3.7 ± 2.5
Minor Axis (μm)	N/A	1.90 ± 0.08	1.7 ± 0.7
Aspect Ratio	N/A	1.40 ± 0.03	2.10 ± 0.02
Interparticle Spacing (μm)	N/A	23.5 ± 1.4	10.9 ± 0.9
Degree of Clustering (Coefficient of Variance of Interparticle Spacing)	N/A	0.40 ± 0.05	0.60 ± 0.03
Sn-Rich Matrix Characteristics			
Dendrite Length (μm)	27.7 ± 10.2	11.3 ± .2	12.9 ± 3.1
Dendrite Spacing (μm)	17.1 ± 5.5	6.7 ± 1.9	7.5 ± 2.4

Rare earths (REs), such as cerium and lanthanum, have been used extensively for microstructural refinement and creep resistance in steel, cast iron, and aluminum alloys.[6–9] Preliminary studies on RE-containing solders, such as Sn-0.7Cu, Sn-Zn, Sn-Ag-Cu, Sn-3.5Ag, and Au-Sn show a discrepancy in reported microstructures and mechanical properties.[10–18] Furthermore, there is little evidence in the literature for the formation of homogeneous microstructures in these RE solders. The variability in microstructures can likely be attributed to a wide variety of processing parameters and procedures.[14] Processing of these materials is particularly important because the high affinity of RE elements with oxygen can lead to oxidation of the RE precursors. In addition to the variability in processing and microstructures, a large discrepancy in mechanical properties is also present in the literature. Some studies report that RE additions increase the strength of Sn-Ag-Cu solders, with an accompanying decrease in strain to failure.[10,11,13,14,16–18] Other studies, however, have reported increases in strain to failure with small amounts of RE.[12,15]

Given the discrepancies in the literature, a thorough study quantifying the microstructure and mechanical properties of RE-containing solder alloys is needed. In particular, special attention needs to be paid to the processing procedures employed and their relationship to microstructure. In this study, the effect of lanthanum additions (0.1 wt.% and 0.5 wt.%) on the microstructure and shear strength of an Sn-3.9Ag-0.7Cu alloy was investigated. Lanthanum was chosen due to its low melting temperature compared to other RE elements, its wide availability, and relatively low cost. It will be

shown that large strain to failures (over 150% increase over conventional Sn-Ag-Cu) can be obtained with relatively small lanthanum additions. This improvement in ductility comes with a very small penalty in shear strength. The relationship between processing, microstructure, and mechanisms for deformation in these materials is discussed in detail.

See the sidebar for details on materials and experimental procedures.

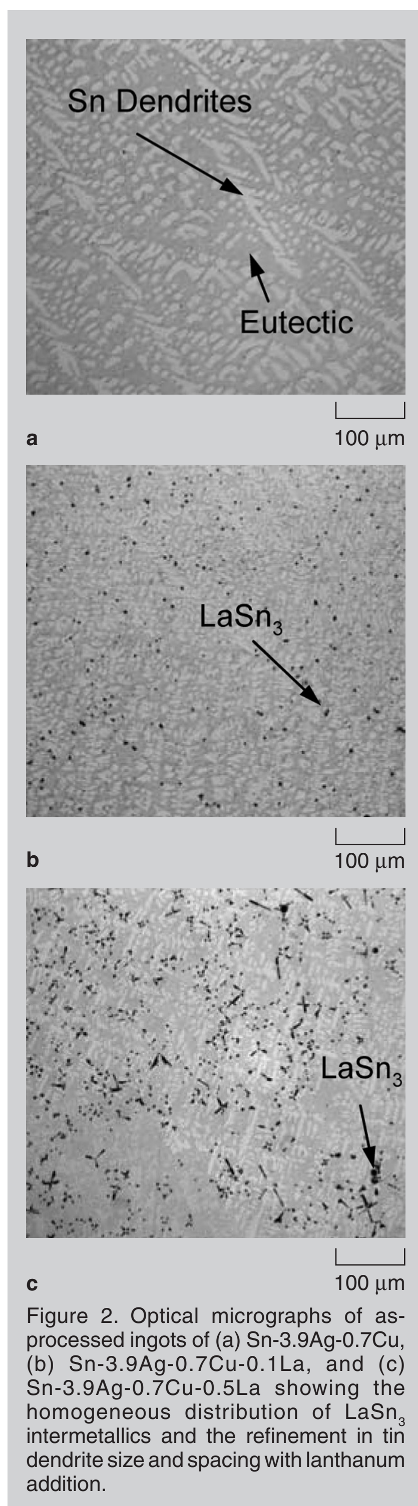

Figure 2. Optical micrographs of as-processed ingots of (a) Sn-3.9Ag-0.7Cu, (b) Sn-3.9Ag-0.7Cu-0.1La, and (c) Sn-3.9Ag-0.7Cu-0.5La showing the homogeneous distribution of $LaSn_3$ intermetallics and the refinement in tin dendrite size and spacing with lanthanum addition.

RESULTS AND DISCUSSION

Differential Scanning Calorimetry

Figure 1 shows the heat flow vs. temperature melting curves obtained from differential scanning calorimetry on heating for Sn-3.9Ag-0.7Cu and Sn-3.9Ag-0.7Cu-0.5La. Both curves show a single melting peak (endothermic), with the onset temperature around 217°C, indicating that lanthanum had little effect on the reflow temperature of the eutectic solder. In the Sn-3.9Ag-0.7Cu-0.5La alloy, however, small peaks can be seen between 325°C and 350°C. Judging by the Sn-La phase diagram, this appears to be a reasonable temperature range for melting of the small amount of $LaSn_3$ (~ 2.5 vol.%). The endothermic peak in the Sn-3.9Ag-0.7Cu-0.5La curve at ~ 335°C indicates that $LaSn_3$ is the primary intermetallic in this alloy, and that at standard reflow temperatures, $LaSn_3$ will remain present in the melt.

Microstructure Characterization

As-Processed Microstructure

Representative microstructures of as-processed Sn-3.9Ag-0.7Cu, Sn-3.9Ag-0.7Cu-0.1La, and Sn-3.9Ag-0.7Cu-0.5La are shown in Figure 2. As expected, the microstructure of near-eutectic Sn-Ag-Cu alloy consisted of tin dendrites and

MATERIALS AND EXPERIMENTAL PROCEDURE

Vacuum-melted ingots of Sn-Ag-Cu with varying amounts of lanthanum (0.1 wt.% and 0.5 wt.%) were prepared. High-purity Sn-3.9Ag-0.7Cu ingots (Indium, Ithaca, New York) were cut into small rectangular pieces (6.5 mm × 6.5 mm × 13 mm) and mixed with lanthanum shot, roughly 2–8 mm^3 in size (ESPI, Ashland, Oregon, 99.995% pure). The materials were mixed in a quartz ampoule (12 mm in diameter) under a sealed glovebox with helium atmosphere. The quartz ampoule was then evacuated to 10^{-5} torr and sealed. The sealed ampoules were heat treated at 1,000°C for 4 h. The ampoules were then water quenched and the samples were removed and sectioned. Microstructure characterization was conducted on the as-processed ingot material as well as after reflow of the solder joints. Ingots were sectioned and polished to a final finish of 0.05 µm colloidal silica. Optical microscopy, scanning-electron microscopy (SEM), transmission-electron microscopy (TEM), and image analysis were conducted to quantify the microstructure. Energy-dispersive spectroscopy (EDS) analysis was also used to confirm the composition of the lanthanum-containing intermetallic. Transmission-electron microscopy sample preparation was conducted by polishing samples to a thickness of about 100 µm, dimpling, and ion milling. Ion milling was conducted using a liquid nitrogen-cooled stage to minimize sample heating. Quantitative microstructure characterization was conducted using image analysis software (ImageJ, Gaithersburg, Maryland) on both optical and SEM micrographs. Details of the microstructure analysis can be found elsewhere.[19] Differential-scanning calorimetry (DSC) was used to determine the melting point of the solder with lanthanum addition. Samples of 20–40 mg were prepared, weighed, and placed into Al_2O_3 crucible pans. An empty Al_2O_3 crucible was used as a reference. Samples were then heated and cooled at a rate of 1°C/min. in the temperature range of 25°C to 600°C.

Mechanical testing was conducted on solder/copper single-lap shear joints. As-processed solder ingots were machined into 6.35 mm × 6.35 mm × 0.5 mm squares. These were lightly polished to remove oxidation caused by the machining process and ultrasonically cleaned in acetone. Oxygen-free copper bars (50.8 mm and 6.35 mm in thickness) were polished to a 0.05 µm finish with colloidal silica solution and etched in 2 vol.% nitric acid for 10 s to remove residual oxides. A graphite mask was applied to the copper bars, leaving a 6.35 mm × 6.35 mm area for reflow. A rosin mildly activated flux was applied to the unmasked portions of the copper bars to improve wetting between the copper and the solder. The joint was assembled with the aid of a reflow fixture to minimize misalignment and maintain a consistent joint solder thickness of approximately 500 µm.[20] The entire assembly was heated on a hot plate and held at 120°C for 20 min. to allow excess flux to vaporize. The temperature was then raised until the solder reached 220°C and was held for 40 s (temperature not exceeding 240°C). The assembly was then removed from the hot plate and air cooled on an aluminum heat sink. The temperature in the solder was monitored using a thermocouple, and a reproducible cooling rate of 0.7°C/s was obtained. The cooling rate was measured from the peak temperature to 150°C, as the joint microstructure does not change significantly below this temperature during cooling.[21–23] Shear testing was conducted using a servo-hydraulic load frame at room temperature and a shear strain rate of 10^{-3} s^{-1}. The strain was measured using an extensometer with a gage length of 10 mm. Fractographic analysis was conducted by SEM.

a eutectic mixture of Ag_3Sn and Cu_6Sn_5 intermetallics distributed in the tin-rich matrix.[24–27] The microstructure of the lanthanum-containing solders consisted of discrete, homogeneously distributed $LaSn_3$ (Figures 2b and c). The Sn-La phase diagram predicts the formation of an intermetallic phase, $LaSn_3$, for tin concentrations greater than 72 wt.% Sn.[28] An analysis of the particles conducted with energy-dispersive spectroscopy yielded an atomic ratio between tin and lanthanum of approximately 3:1, confirming the composition of the particles as $LaSn_3$.

In the lanthanum-containing solders, the $LaSn_3$ intermetallics had a characteristic faceted geometry (Figure 3a) also referred to as "Chinese scripts," which have also been observed in other systems.[29–32] A recent analysis by Dudek and Chawla[33] using three-dimensional visualization techniques showed that the $LaSn_3$ intermetallics are actually complex dendrites (Figure 3b). The microstructure shown in in Figure 3b is from a slow-cooled sample, so the size of the dendrites is much larger than that shown in Figure 2.

It was discovered that a high degree of interconnected porosity exists within the dendritic structures (Figure 3c). Serial sectioning of two-dimensional (2-D) microstructural images with computer-aided reconstruction and visualization has been used to visualize and quantify intermetallics in other lead-free solder systems.[34,35] Details regarding the experimental approach for the 3-D reconstruction process using serial sectioning can be obtained elsewhere.[33] The formation of the faceted intermetallic geometry can be attributed to a combination of factors. These include solid/liquid interface stability during diffusional growth, the orientation dependence of interface energy (i.e., certain growth planes will dominate to minimize total surface energy), and the minimization of strain energy due to volume changes associated with differences in structure and bonding between solid and liquid phases.[36]

The $LaSn_3$ phases are considerably larger in size than the other intermetallic phases, are present in the eutectic, and surround the boundaries of the tin dendrites. Figure 2 clearly shows that there is some microstructural refinement of

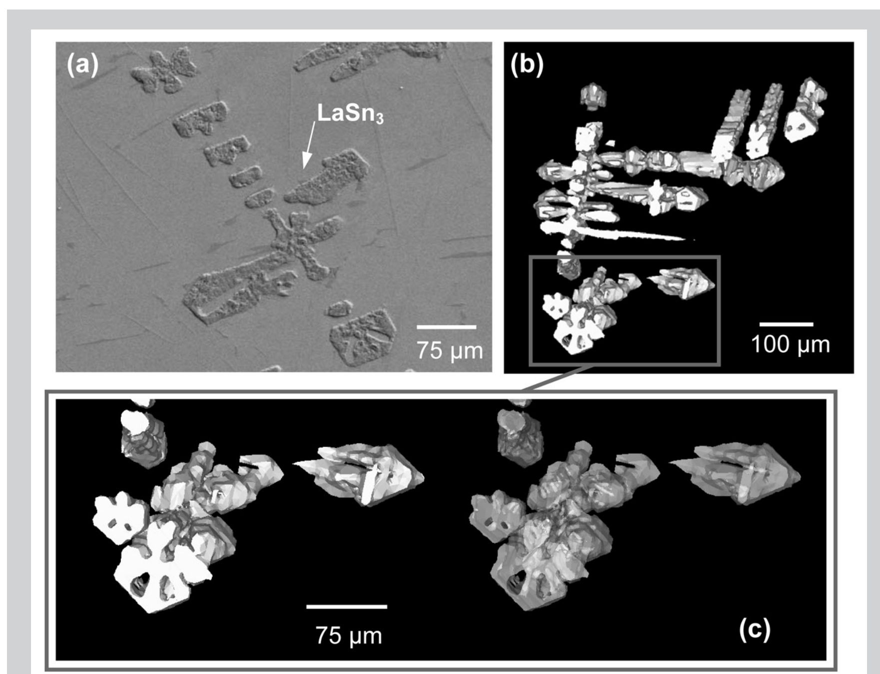

Figure 3. (a) A backscattered SEM micrograph of Sn-3.9Ag-0.7Cu-0.5La alloy showing the $LaSn_3$ intermetallics; (b) a three-dimensional microstructure reconstructed from serial sections, highlighting the complex dendritic morphology of the $LaSn_3$;[19] and (c) a high-magnification image showing the presence of interconnected porosity within the dendritic structure.

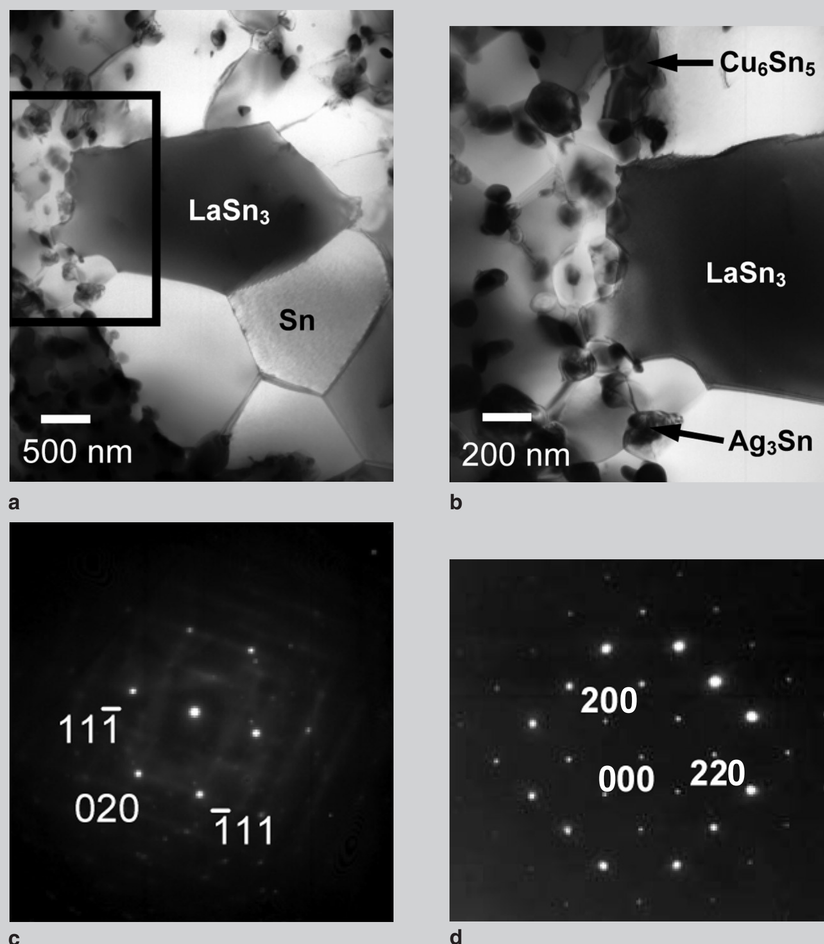

Figure 4. Transmission-electron micrographs and diffraction patterns from as-processed (a) Sn-3.9Ag-0.7Cu-0.5La and (b) showing the eutectic microstructure consisting of Ag_3Sn and Cu_6Sn_5 intermetallics surrounded by a tin matrix, and dendritic tin grains nucleating from the faceted edges of the $LaSn_3$ intermetallic diffraction patterns for (c) $LaSn_3$, showing an $L1_2$ crystal structure and (d) tin, showing its BCT crystal structure.

Table II. Summary of Microstructure Characterization for Reflowed Solder Joint Systems

	Concentration of La (wt.%)		
	0	0.1	0.5
$LaSn_3$ Characteristics			
Major Axis (μm)	N/A	2.9 ± 0.3	3.9 ± 2.1
Minor Axis (μm)	N/A	1.7 ± 0.1	1.4 ± 0.9
Aspect Ratio	N/A	1.7 ± 0.1	2.7 ± 0.1
Interparticle Spacing (μm)	N/A	20.3 ± 1.5	10.9 ± 0.9
Degree of Clustering (Coefficient of Variance of Interparticle Spacing)	N/A	0.41 ± 0.06	0.62 ± 0.04
Sn-Rich Matrix Characteristics			
Sn Secondary Dendrite Length (μm)	41.8 ± 39.5	14.0 ± 4.9	20.5 ± 12.1
Sn Secondary Dendrite Spacing (μm)	12.6 ± 5.3	11.2 ± 3.1	9.0 ± 3.2
Joint Characteristics			
Cu_6Sn_5 Intermetallic Thickness (μm)	5.5 ± 1.6	2.1 ± 0.4	2.7 ± 0.8

the tin matrix in the lanthanum-containing alloys compared with the base Sn-Ag-Cu alloy. This is exemplified by the quantitative measurements shown in Table I. At 0.5 wt.% La, for example, the tin dendrite length is approximately 60% smaller than for 0 wt.%. A comparison of Sn-3.9Ag-0.7Cu-0.1La and Sn-3.9Ag-0.7Cu-0.5La shows that the size and distribution of $LaSn_3$ intermetallics differ. Sn-3.9Ag-0.7Cu-0.1La has smaller $LaSn_3$ particles which are more homogeneously distributed, as seen from the coefficient of variance analysis.

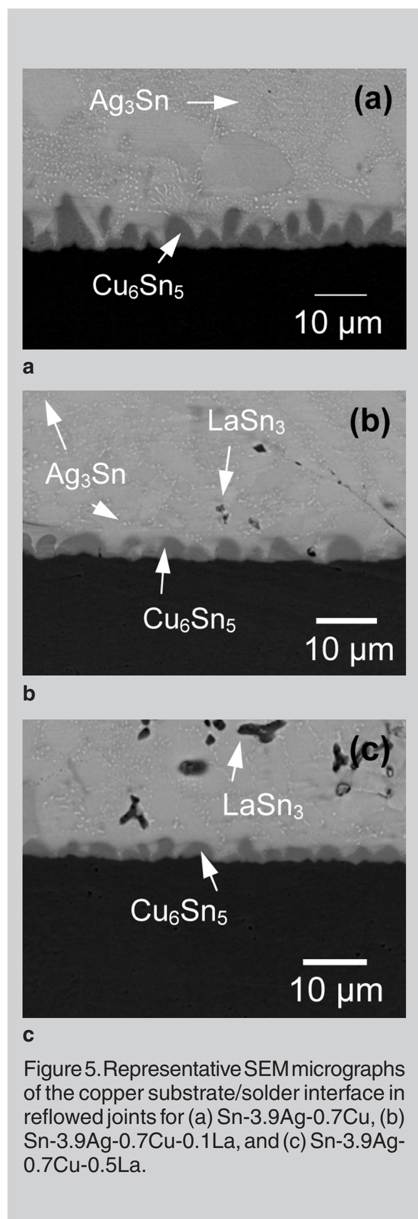

Figure 5. Representative SEM micrographs of the copper substrate/solder interface in reflowed joints for (a) Sn-3.9Ag-0.7Cu, (b) Sn-3.9Ag-0.7Cu-0.1La, and (c) Sn-3.9Ag-0.7Cu-0.5La.

Details regarding the solidification pathway for the lanthanum-containing solders have been reported elsewhere.[19] Note that from TEM analysis (Figure 4), one can deduce that the tin grains are in fact nucleating and growing from the faceted edges of the $LaSn_3$ intermetallics. The large amount of heterogeneous nucleation sites provided by the $LaSn_3$ appear to explain the decrease in size of tin dendrites in the lanthanum-containing solders observed in Figure 2.

Reflowed Microstructure

The microstructures of the joints are coarser than that of the as-processed material due to the somewhat slower cooling rate, which allows more time for tin-dendrite and intermetallic growth. The Ag_3Sn particles exhibited a spherical morphology, similar in size to that in the as-processed material. Relatively large Cu_6Sn_5 particles (~25 μm) were also observed in the eutectic region. Table II shows quantitative measurements of $LaSn_3$ and Ag_3Sn size and aspect ratio. It also shows measurements of tin dendrite size and dendrite arm spacing. A comparison to Table I, which contains measurements in the as-processed condition, shows that the $LaSn_3$ intermetallics do not undergo significant coarsening or segregation during the reflow process (relative to the as-processed condition). This is expected, since the reflow temperature is not high enough to melt the $LaSn_3$ intermetallics. Note that the lanthanum-containing solders still have a finer tin dendrite structure after reflow when compared with the Sn-Ag-Cu base material.

The interface between the solder and copper substrate for all alloys is characterized by the formation of a thin Cu_6Sn_5 intermetallic layer upon reflow[20,37] (Figure 5). This intermetallic layer is characterized by a nodular or planar morphology.[20,23,38] It is interesting to note that in the lanthanum-containing alloys, the intermetallic thickness has decreased by approximately 60% compared with the Sn-Ag-Cu alloy. This result could have a substantial impact on the mechanical behavior of the joints, since the thickness of this intermetallic layer affects the properties of solder/copper joints.[39]

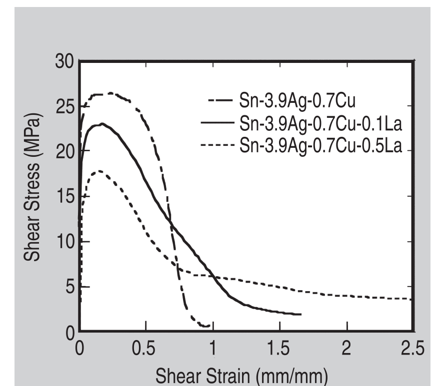

Figure 6. The shear stress vs. shear strain curves for Sn-3.9Ag-0.7Cu, Sn-3.9Ag-0.7Cu-0.1La, and Sn-3.9Ag-0.7Cu-0.5La tested in monotonic shear.

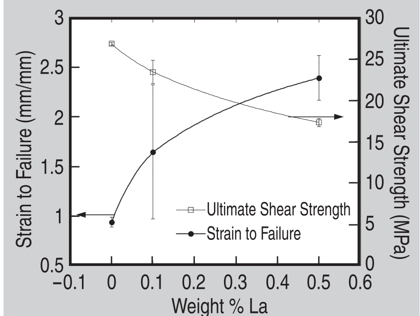

Figure 7. The ultimate shear strength and strain to failure for monotonic shear testing vs. weight percent lanthanum, showing asymptotic relationships indicating the presence of a critical lanthanum concentration for decreasing shear strength and improving ductility.

Shear Behavior

The shear behavior of Sn-3.9Ag-0.7Cu, Sn-3.9Ag-0.7Cu-0.1La, and Sn-3.9Ag-0.7Cu-0.5La is shown in Figure 6. Table III summarizes the shear behavior of the joints. The ultimate shear strength decreased slightly with increasing lanthanum concentration (Figure 7). The lanthanum-containing alloys are quite damage tolerant in nature, given that the decrease in stress after the ultimate shear strength is quite gradual and not abrupt (as is the case for Sn-Ag-Cu). The strain-to-failure was taken as a deviation of 5% from a linear regression fit to the end of the stress-strain curve.[19] More importantly, the strain to failure of Sn-3.9Ag-0.7Cu-0.5La samples increased significantly, nearly 150%, over that of Sn-3.9Ag-0.7Cu (Figure 7).

Table III. Monotonic Shear Results for Sn-3.9Ag-0.7Cu, Sn-3.9Ag-0.7Cu-0.1La, and Sn-3.9Ag-0.7Cu-0.5La

Alloy	Ultimate Shear Strength (MPa)	Strain to Failure (%)
Sn-3.9Ag-0.7Cu	26.8 ± 0.2	94 ± 5
Sn-3.9Ag-0.7Cu-0.1La	23.4 ± 1.4	164 ± 67
Sn-3.9Ag-0.7Cu-0.5La	17.3 ± 0.5	239 ± 22

Examination of the fractured surfaces of the joints (Figure 8) revealed a classical void nucleation, growth, and coalescence process in the Sn-3.9Ag-0.7Cu-0.5La, where the bottom of most dimples contained $LaSn_3$ intermetallics. Note that fracture occurred through the solder, away from the Cu_6Sn_5 intermetallic/solder interface. The resulting fracture path was relatively tortuous in nature, with visible steps on the fracture surface. Sn-3.9Ag-0.7Cu exhibited more of a tearing type of fracture morphology with feature sizes (voids developed during fracture) that were much smaller than that in Sn-3.9Ag-0.7Cu-0.5La. Fracture in Sn-3.9Ag-0.7Cu occurred at the interfacial region between the solder and the Cu_6Sn_5 intermetallic, exposing the tips of the Cu_6Sn_5 nodules in some areas.[20] Sn-3.9Ag-0.7Cu-0.1La appears to behave more similarly to Sn-3.9Ag-0.7Cu, with fracture also occurring along the interfacial region. Voids caused by the fracture process are also smaller in scale than for the Sn-3.9Ag-0.7Cu-0.5La joints, although there is evidence for the presence of $LaSn_3$ at the base of the voids.

The authors believe that the increase in ductility with increasing lanthanum concentration is caused by the ability of the $LaSn_3$ intermetallics to nucleate and grow voids in the solder interior, dominating the fracture process and minimizing crack growth along the brittle Cu_6Sn_5 intermetallic/solder interface. Figure 9 is a schematic of the likely fracture mode for the lanthanum-containing solders. Crack propagation along the intermetallic interface in the 0.5 wt.% lanthanum-containing samples does not take place. This is likely a result of stresses within the solder being more homogeneously distributed and not concentrated at the intermetallic/solder interface. Thus, in Sn-Ag-Cu, fracture is localized to a very small fraction of the joint. The addition of lanthanum, however, allows deformation to be "spread out" over the entire joint volume, which results in a higher macroscopic ductility.

CONCLUSION

The enhanced ductility observed by these La-containing solders has profound implications for improving the mechanical shock resistance (such as drop failure) of electronic packages containing Sn-Ag-Cu solders. This enhancement could lead to increased reliability of portable devices. In addition, the unique microstructures and melting characteristics of the $LaSn_3$ phase provides us with the

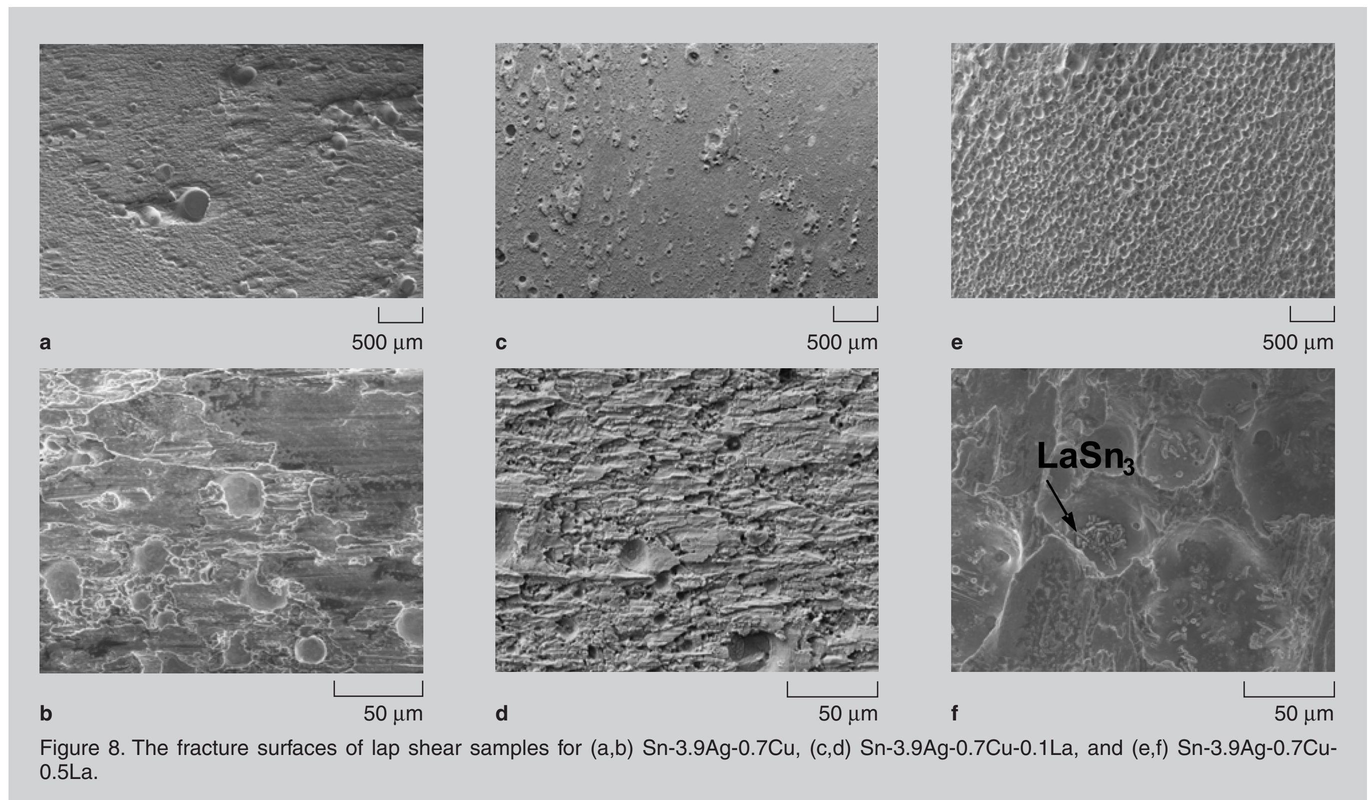

Figure 8. The fracture surfaces of lap shear samples for (a,b) Sn-3.9Ag-0.7Cu, (c,d) Sn-3.9Ag-0.7Cu-0.1La, and (e,f) Sn-3.9Ag-0.7Cu-0.5La.

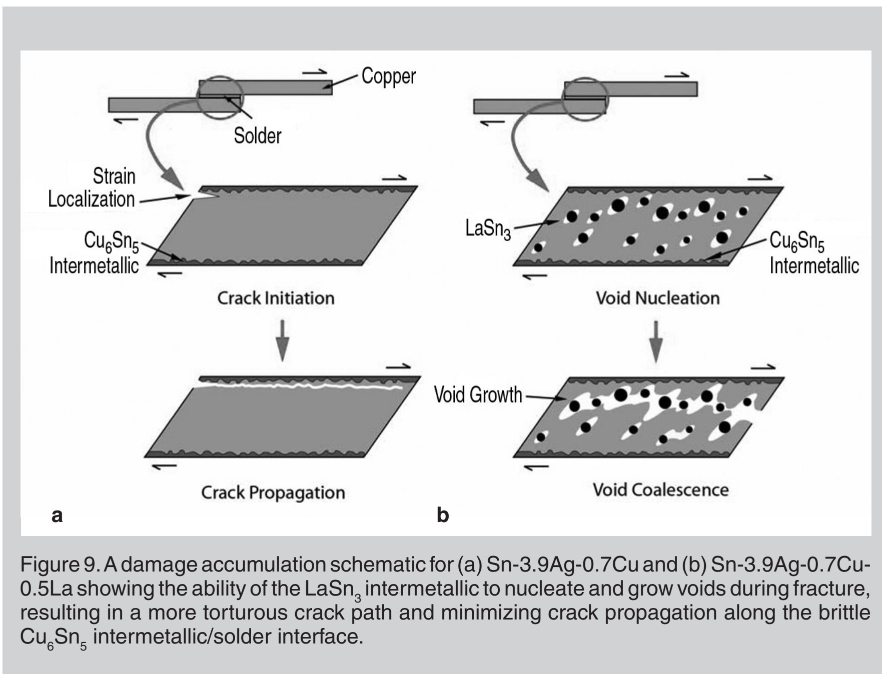

Figure 9. A damage accumulation schematic for (a) Sn-3.9Ag-0.7Cu and (b) Sn-3.9Ag-0.7Cu-0.5La showing the ability of the $LaSn_3$ intermetallic to nucleate and grow voids during fracture, resulting in a more torturous crack path and minimizing crack propagation along the brittle Cu_6Sn_5 intermetallic/solder interface.

ability to tailor the mechanical properties, and develop new tin-rich lead-free solder systems with unique properties.

ACKNOWLEDGEMENTS

The authors gratefully acknowledge financial support for this research from the Semiconductor Research Corporation under contract #2005-KJ-1286 (Dr. M. Renavikar, Intel, industrial liaison, and Dr. H. Hosack, program manager). The authors also thank David Wright from the Center for Solid State Science, Arizona State University for his assistance with evacuating the quartz tubes.

References

1. J. Bath, C. Handwerker, and E. Bradley, *Circ Assemb.* 11 (5) (2000), pp. 30–40.
2. I.E. Anderson et al., *J. Electron. Mater.*, 30 (2001), pp. 1050–1059.
3. D.H. Kim, P. Elenius, and S. Barrett, *IEEE Trans. Electron. Pack. Manu.,* 25 (2) (2002), pp. 84–90.
4. M.E. Loomans and M.E. Fine, *Metall. Mater. Trans. A,* 31 (4) (2000), pp. 1155–1162.
5. A. Schubert et al., *Proceedings International Symposium on Advanced Packaging Materials Processes, Properties and Interfaces* (Piscataway, NJ: IEEE, 2001), pp. 129–134.
6. D.H. Xiao et al., *J. Alloy Compd.,* 352 (2003), pp. 84–88.
7. J.O. Choi et al., *Mat. Sci. Eng. A-Struc.*, 383 (2004), pp. 323–333.
8. G. Pettersen et al., *Mat. Sci. Eng. A-Struc.,* 207 (1996), pp. 115–120.
9. J. Chang, I. Moon, and C. Choi, *J. Mater. Sci.*, 33 (1998), pp. 5015–5023.
10. A. Ramirez, H. Mavoori, and S. Jin, *Appl. Phys. Lett.*, 80 (3) (2002), pp. 398–400.
11. C.M.K. Wu et al., *J. Electron. Mater.*, 32 (2) (2003), pp. 63–69.
12. Z.G. Chen et al., *J. Electron. Mater.*, 32 (4) (2003), pp. 235–243.
13. D.Q. Yu, J. Zhao, and L. Wang, *J. Alloy. Compd.*, 376 (2004), pp. 170–175.
14. Z. Xia et al., *J. Electron. Mater.,* 31 (6) (2002), pp. 564–567.
15. Z.G. Chen et al., *J. Electron. Mater.*, 31 (10) (2002), pp. 1122–1128.
16. C.M.T. Law et al., *IEEE Transactions on Advanced Packaging,* 28 (2) (2005), pp. 252–258.
17. C.M.L. Wu et al., *Mater. Res.*, 17 (12) (2002), pp. 3146–3154.
18. X. Ma, Y. Qian, and F. Yoshida, *J. Rare Earth,* 18 (4) (2000), pp. 289–292.
19. M.A. Dudek et al., *J. Electron. Mater.,* (2006) in press..
20. X. Deng et al., *Metall. Mater. Trans. A,* 36A (1) (2005), pp. 55–64.
21. F. Ochoa, X. Deng, and N. Chawla, *J. Electron. Mater.,* 33 (2004), pp. 1596–1607.
22. N. Chawla et al., *J. Mater. Sci.-Mater. Electron.*, 15 (2004), pp. 385–388.
23. X. Deng et al., *J. Electron. Mater.*, 32 (2003), pp. 1403–1413.
24. K.W. Moon et al., *J. Electron. Mater.,* 29 (2000), pp. 1122–1136.
25. D.R. Frear, *Mechanics of Solder Alloy Interconnects* (New York: Van Nostran, 1994).
26. S. Kang and A.K. Sarkhel, *J. Electron. Mater.*, 23 (1994), pp. 701–707.
27. J. Glazer, *Int. Mater. Rev.*, 40 (1995), pp. 65–93.
28. H. Okamoto, editor, *Phase Diagrams for Binary Alloys* (Materials Park, OH: ASM, 2000).
29. S. Beer, G. Frommeyer, and E. Schmid, *Proc. Conf. Magnesium Alloys and their Applications* (Frankfurt: DGM Informationsgesellschaft m.b.H., 1992), pp. 317–324.
30. Y.N. Malinochka, L.N. Bagnyuk, and S.A. Zdorovets, *Russ. Metall.,* 1 (1989), pp. 76–83.
31. R. Kesri and S. Hamar-Thibault, *Zeitschrift fuer Metallkunde*, 80 (7) (1989), pp. 502–510.
32. K. Ichikawa and S. Ishizuka, *T. Jpn. I. Met.,* 30 (1) (1990), pp. 75–82.
33. M.A. Dudek and N. Chawla, *Mater. Charac.,* (2006), in preparation.
34. R.S. Sidhu and N. Chawla, *Mater. Charac.*, 52 (3) (2004), pp. 225–230.
35. R.S. Sidhu and N. Chawla, *Scripta Mater.*, 54 (9) (2006), pp. 1627–1631.
36. W. Kurz and D.J. Fisher, *Fundamentals of Solidification* (Switzerland: Trans Tech. Publications Ltd., 1998).
37. P.G. Harris and K.S. Chagger, *Solder. Surf. Mt. Tech.*, 10 (3) (1998), p. 38.
38. R.S. Sidhu, X. Deng, and N. Chawla, *Metall. Mater. Trans. A* (2006), submitted.
39. N. Chawla and R.S. Sidhu, *J. Mater. Sci.- Mater. Elect.* (2006), in press.

M.A. Dudek, R.S. Sidhu, and N. Chawla are with the Mechanical Behavior of Materials Facility, Department of Chemical and Materials Engineering, Fulton School of Engineering at Arizona State University in Tempe, Arizona.

For more information, contact Nik Chawla, Arizona State University, Department of Chemical and Materials Engineering, Fulton School of Engineering, Box 876006, Tempe, AZ 85287-6006; (480) 965-2402; fax (480) 965-0037; e-mail nchawla@asu.edu.

Read *JOM* On-Line . . . Just Like You Do in Print!

I've flipped over JOM. Have you?

Turn the Pages, Click the Links at: *http://www.tms.org/JOMPT*